Polarization microscopy for characterizing fiber orientation of ocular tissues

Ning-Jiun Jan,[1,2,3,4] Jonathan L. Grimm,[2,3] Huong Tran,[1,2,3,4] Kira L. Lathrop,[1,2,4] Gadi Wollstein,[2,3,4] Richard A. Bilonick,[1] Hiroshi Ishikawa,[2,3,4] Larry Kagemann,[1,2,3,4] Joel S. Schuman,[1,2,3,4] and Ian A. Sigal[1,2,3,4,*]

[1]Department of Bioengineering, Swanson School of Engineering, University of Pittsburgh, Pittsburgh, Pennsylvania, USA
[2]UPMC Eye Center, Eye and Ear Institute, Ophthalmology and Visual Science Research Center, Department of Ophthalmology, University of Pittsburgh School of Medicine, Pittsburgh, Pennsylvania, USA
[3]McGowan Institute for Regenerative Medicine, University of Pittsburgh School of Medicine and University of Pittsburgh, Pittsburgh, Pennsylvania, USA
[4]The Louis J. Fox Center for Vision Restoration of UPMC and the University of Pittsburgh, Pittsburgh, PA, USA
*ian@ocularbiomechanics.com

Abstract: Characterizing the collagen fiber orientation and organization in the eye is necessary for a complete understanding of ocular biomechanics. In this study, we assess the performance of polarized light microscopy to determine collagen fiber orientation of ocular tissues. Our results demonstrate that the method provides objective, accurate, repeatable and robust data on fiber orientation with µm-scale resolution over a broad, cm-scale, field of view, unaffected by formalin fixation, without requiring tissue dehydration, labeling or staining. Together, this shows that polarized light microscopy is a powerful method for studying collagen architecture in the eye, with applications ranging from normal physiology and aging, to pathology and transplantation.

References and links

1. R. C. Pruett, "Progressive myopia and intraocular pressure: what is the linkage? A literature review," Acta Ophthalmol. Suppl. **185**(S185), 117–127 (1988).
2. I. A. Sigal and C. R. Ethier, "Biomechanics of the optic nerve head," Exp. Eye Res. **88**(4), 799–807 (2009).
3. M. Romero-Jiménez, J. Santodomingo-Rubido, and J. S. Wolffsohn, "Keratoconus: a review," Cont. Lens Anterior Eye **33**(4), 157–166 (2010).
4. M. J. A. Girard, W. J. Dupps, M. Baskaran, G. Scarcelli, S. H. Yun, H. A. Quigley, I. A. Sigal, and N. G. Strouthidis, "Translating ocular biomechanics into clinical practice: current state and future prospects," Curr. Eye Res. **40**(1), 1–18 (2015).
5. P. G. Watson and R. D. Young, "Scleral structure, organisation and disease. A review," Exp. Eye Res. **78**(3), 609–623 (2004).
6. K. M. Meek and N. J. Fullwood, "Corneal and scleral collagens--a microscopist's perspective," Micron **32**(3), 261–272 (2001).
7. M. J. A. Girard, A. Dahlmann-Noor, S. Rayapureddi, J. A. Bechara, B. M. E. Bertin, H. Jones, J. Albon, P. T. Khaw, and C. R. Ethier, "Quantitative mapping of scleral fiber orientation in normal rat eyes," Invest. Ophthalmol. Vis. Sci. **52**(13), 9684–9693 (2011).
8. D. Yan, S. McPheeters, G. Johnson, U. Utzinger, and J. P. Vande Geest, "Microstructural differences in the human posterior sclera as a function of age and race," Invest. Ophthalmol. Vis. Sci. **52**(2), 821–829 (2011).
9. K. M. Meek and C. Boote, "The use of X-ray scattering techniques to quantify the orientation and distribution of collagen in the corneal stroma," Prog. Retin. Eye Res. **28**(5), 369–392 (2009).
10. J. K. Pijanka, B. Coudrillier, K. Ziegler, T. Sorensen, K. M. Meek, T. D. Nguyen, H. A. Quigley, and C. Boote, "Quantitative mapping of collagen fiber orientation in non-glaucoma and glaucoma posterior human sclerae," Invest. Ophthalmol. Vis. Sci. **53**(9), 5258–5270 (2012).
11. B. Coudrillier, C. Boote, H. A. Quigley, and T. D. Nguyen, "Scleral anisotropy and its effects on the mechanical response of the optic nerve head," Biomech. Model. Mechanobiol. **12**(5), 941–963 (2013).

12. B. Coudrillier, R. L. Abel, J. Albon, I. C. Campbell, and C. R. Ethier, "Micro-computed Tomography (μCT) for the Structural Analysis of the Lamina Cribrosa (LC)," Invest. Ophthalmol. Vis. Sci. **55**(13), 4253 (2014).
13. N. Morishige, A. J. Wahlert, M. C. Kenney, D. J. Brown, K. Kawamoto, T. Chikama, T. Nishida, and J. V. Jester, "Second-harmonic imaging microscopy of normal human and keratoconus cornea," Invest. Ophthalmol. Vis. Sci. **48**(3), 1087–1094 (2007).
14. D. J. Brown, N. Morishige, A. Neekhra, D. S. Minckler, and J. V. Jester, "Application of second harmonic imaging microscopy to assess structural changes in optic nerve head structure ex vivo," J. Biomed. Opt. **12**(2), 024029 (2007).
15. K. M. Mountain, T. A. Bjarnason, J. F. Dunn, and J. R. Matyas, "The functional microstructure of tendon collagen revealed by high-field MRI," Magn. Reson. Med. **66**(2), 520–527 (2011).
16. L. C. Ho, I. A. Sigal, N.-J. Jan, A. Squires, Z. Tse, E. X. Wu, S.-G. Kim, J. S. Schuman, and K. C. Chan, "Magic Angle-Enhanced MRI of Fibrous Microstructures in Sclera and Cornea With and Without Intraocular Pressure Loading," Invest. Ophthalmol. Vis. Sci. **55**(9), 5662–5672 (2014).
17. M. J. A. Girard, J. C. Downs, M. Bottlang, C. F. Burgoyne, and J. K. F. Suh, "Peripapillary and posterior scleral mechanics--part II: experimental and inverse finite element characterization," J. Biomech. Eng. **131**(5), 051012 (2009).
18. R. Grytz, G. Meschke, and J. B. Jonas, "The collagen fibril architecture in the lamina cribrosa and peripapillary sclera predicted by a computational remodeling approach," Biomech. Model. Mechanobiol. **10**(3), 371–382 (2011).
19. C. R. Ethier, M. Johnson, and J. Ruberti, "Ocular biomechanics and biotransport," Annu. Rev. Biomed. Eng. **6**(1), 249–273 (2004).
20. S. E. Szczesny, J. M. Peloquin, D. H. Cortes, J. A. Kadlowec, L. J. Soslowsky, and D. M. Elliott, "Biaxial tensile testing and constitutive modeling of human supraspinatus tendon," J. Biomech. Eng. **134**(2), 021004 (2012).
21. J. Diamant, A. Keller, E. Baer, M. Litt, and R. G. C. Arridge, "Collagen; ultrastructure and its relation to mechanical properties as a function of ageing," Proc. R. Soc. Lond. B Biol. Sci. **180**(1060), 293–315 (1972).
22. K. Komatsu, L. Mosekilde, A. Viidik, and M. Chiba, "Polarized light microscopic analyses of collagen fibers in the rat incisor periodontal ligament in relation to areas, regions, and ages," Anat. Rec. **268**(4), 381–387 (2002).
23. N. M. Kalwani, C. A. Ong, A. C. Lysaght, S. J. Haward, G. H. McKinley, and K. M. Stankovic, "Quantitative polarized light microscopy of unstained mammalian cochlear sections," J. Biomed. Opt. **18**(2), 026021 (2013).
24. R. H. Newton, J. Y. Brown, and K. M. Meek, "Polarized light microscopy technique for quantitatively mapping collagen fibril orientation in cornea," in *BiOS Europe'96*, (International Society for Optics and Photonics, 1996), 278–284.
25. G. P. Misson, "Circular polarization biomicroscopy: a method for determining human corneal stromal lamellar organization in vivo," Ophthalmic Physiol. Opt. **27**(3), 256–264 (2007).
26. M. Nordin and V. H. Frankel, *Basic Biomechanics of the Musculoskeletal System* (Lippincott Williams & Wilkins, 2001).
27. J. K. Pijanka, M. T. Spang, T. Sorensen, J. Liu, T. D. Nguyen, H. A. Quigley, and C. Boote, "Depth-Dependent Changes in Collagen Organization in the Human Peripapillary Sclera," PLoS One **10**(2), e0118648 (2015).
28. K. M. Meek and C. Boote, "The organization of collagen in the corneal stroma," Exp. Eye Res. **78**(3), 503–512 (2004).
29. J. W. Ruberti and J. D. Zieske, "Prelude to corneal tissue engineering - gaining control of collagen organization," Prog. Retin. Eye Res. **27**(5), 549–577 (2008).
30. J. Schindelin, I. Arganda-Carreras, E. Frise, V. Kaynig, M. Longair, T. Pietzsch, S. Preibisch, C. Rueden, S. Saalfeld, B. Schmid, J. Y. Tinevez, D. J. White, V. Hartenstein, K. Eliceiri, P. Tomancak, and A. Cardona, "Fiji: an open-source platform for biological-image analysis," Nat. Methods **9**(7), 676–682 (2012).
31. R. A. Bouhenni, J. Dunmire, A. Sewell, and D. P. Edward, "Animal models of glaucoma," J. Biomed. Biotechnol. **2012**, 692609 (2012).
32. K. A. Hansen, J. A. Weiss, and J. K. Barton, "Recruitment of Tendon Crimp With Applied Tensile Strain," J. Biomech. Eng. **124**(1), 72–77 (2002).
33. M. Franchi, M. Fini, M. Quaranta, V. De Pasquale, M. Raspanti, G. Giavaresi, V. Ottani, and A. Ruggeri, "Crimp morphology in relaxed and stretched rat Achilles tendon," J. Anat. **210**(1), 1–7 (2007).
34. I. A. F. Stokes, C. McBride, D. D. Aronsson, and P. J. Roughley, "Intervertebral disc changes with angulation, compression and reduced mobility simulating altered mechanical environment in scoliosis," Eur. Spine J. **20**(10), 1735–1744 (2011).
35. M. R. Hill, X. Duan, G. A. Gibson, S. Watkins, and A. M. Robertson, "A theoretical and non-destructive experimental approach for direct inclusion of measured collagen orientation and recruitment into mechanical models of the artery wall," J. Biomech. **45**(5), 762–771 (2012).
36. X. Liu, L. Wang, J. Ji, W. Yao, W. Wei, J. Fan, S. Joshi, D. Li, and Y. Fan, "A Mechanical Model of the Cornea Considering the Crimping Morphology of Collagen Fibrils," Invest. Ophthalmol. Vis. Sci. **55**(4), 2739–2746 (2014).
37. M. Winkler, G. Shoa, Y. Xie, S. J. Petsche, P. M. Pinsky, T. Juhasz, D. J. Brown, and J. V. Jester, "Three-dimensional distribution of transverse collagen fibers in the anterior human corneal stroma," Invest. Ophthalmol. Vis. Sci. **54**(12), 7293–7301 (2013).
38. D. G. Lowe, "Distinctive image features from scale-invariant keypoints," Int. J. Comput. Vis. **60**(2), 91–110 (2004).

39. S. Preibisch, S. Saalfeld, and P. Tomancak, "Globally optimal stitching of tiled 3D microscopic image acquisitions," Bioinformatics **25**(11), 1463–1465 (2009).
40. F. Helmchen and W. Denk, "Deep tissue two-photon microscopy," Nat. Methods **2**(12), 932–940 (2005).
41. C. P. Neu and G. M. Genin, *Handbook of Imaging in Biological Mechanics* (CRC Press, 2014).
42. M. F. G. Wood, N. Vurgun, M. A. Wallenburg, and I. A. Vitkin, "Effects of formalin fixation on tissue optical polarization properties," Phys. Med. Biol. **56**(8), N115–N122 (2011).
43. M. D. Roberts, V. Grau, J. Grimm, J. Reynaud, A. J. Bellezza, C. F. Burgoyne, and J. C. Downs, "Remodeling of the connective tissue microarchitecture of the lamina cribrosa in early experimental glaucoma," Invest. Ophthalmol. Vis. Sci. **50**(2), 681–690 (2009).
44. S. E. Szczesny and D. M. Elliott, "Evidence for Interfibrillar Shear Load Transfer Between Sliding Fibrils in Tendon," in *ASME 2013 Summer Bioengineering Conference*, (American Society of Mechanical Engineers, 2013), V01BT48A006–V001BT048A006.
45. J. B. Jonas, K. A. Königsreuther, and G. O. H. Naumann, "Optic disc histomorphometry in normal eyes and eyes with secondary angle-closure glaucoma. II. Parapapillary region," Graefes Arch. Clin. Exp. Ophthalmol. **230**(2), 134–139 (1992).
46. J. Albon, W. S. Karwatowski, N. Avery, D. L. Easty, and V. C. Duance, "Changes in the collagenous matrix of the aging human lamina cribrosa," Br. J. Ophthalmol. **79**(4), 368–375 (1995).
47. A. J. Quantock, M. Winkler, G. J. Parfitt, R. D. Young, D. J. Brown, C. Boote, and J. V. Jester, "From nano to macro: studying the hierarchical structure of the corneal extracellular matrix," Exp. Eye Res. **133**, 81–99 (2015).
48. R. Rezakhaniha, A. Agianniotis, J. T. C. Schrauwen, A. Griffa, D. Sage, C. V. Bouten, F. N. van de Vosse, M. Unser, and N. Stergiopulos, "Experimental investigation of collagen waviness and orientation in the arterial adventitia using confocal laser scanning microscopy," Biomech. Model. Mechanobiol. **11**(3-4), 461–473 (2012).
49. C. Boote, S. Dennis, R. H. Newton, H. Puri, and K. M. A. Meek, "Collagen fibrils appear more closely packed in the prepupillary cornea: optical and biomechanical implications," Invest. Ophthalmol. Vis. Sci. **44**(7), 2941–2948 (2003).
50. J. K. Pijanka, A. Abass, T. Sorensen, A. Elsheikh, and C. Boote, "A wide-angle X-ray fibre diffraction method for quantifying collagen orientation across large tissue areas: application to the human eyeball coat," J. Appl. Cryst. **46**(5), 1481–1489 (2013).
51. I. A. Sigal, J. L. Grimm, N.-J. Jan, K. Reid, D. S. Minckler, and D. J. Brown, "Eye-specific IOP-induced displacements and deformations of human lamina cribrosa," Invest. Ophthalmol. Vis. Sci. **55**(1), 1–15 (2014).
52. I. A. Sigal, J. G. Flanagan, I. Tertinegg, and C. R. Ethier, "3D morphometry of the human optic nerve head," Exp. Eye Res. **90**(1), 70–80 (2010).

1. Introduction

Several leading causes of visual impairment such as myopia [1], glaucoma [2], and keratoconus [3] are associated with abnormal ocular connective tissues [4]. Hence, to preserve vision, it is important to characterize two elements central to connective tissues, namely the orientation and organization of the collagen fibers that form them [5, 6]. Several techniques have been developed for measuring collagen fiber orientation and organization, including small angle light scattering [7, 8], x-ray scattering [9–12], non-linear microscopy [7, 13, 14] and magnetic resonance imaging [15, 16], or for estimating them using inverse numerical methods [17, 18]. The complexity of the eye calls for a technique that provides data at multiple scales, including high resolution (micron-scale) and broad field of view (several mm to cm) [19]. The techniques mentioned above, however, are not fully satisfactory because they lack the resolution or field of view, are slow and subjective (e.g. requiring manual fiber tracings), or are susceptible to artifacts (e.g. due to the presence of pigment).

We hypothesized that polarized light microscopy (PLM) would overcome these obstacles and prove a valuable technique for use in ophthalmology. PLM has been proven effective to characterize collagen of tendons [20, 21], ligaments [22] and other soft tissues [23]. The possibility of using PLM in the cornea was discussed almost two decades ago for ex-vivo tissues [24], and more recently to study the cornea stroma in vivo [25]. However, the accuracy, repeatability and robustness of the technique when applied to ocular tissues remains to be determined. Tendon and ligaments are generally similar to collagenous ocular tissues in terms of extracellular matrix composition [26], but there are differences in their structural hierarchies [9] and overall organization [4, 27–29]. Therefore, it cannot be taken for granted that PLM will apply to ocular tissues as it does to other tissues, and the performance of the technique must be assessed. Our goals were to quantify the accuracy, repeatability and robustness of PLM to measure micron-scale collagen fiber orientation of ocular tissues,

demonstrate that this can be achieved with broad, cm-scale, field of view, and thus establish PLM as a technique that yields objective information on the microstructure of the eye.

2. Methods

Below, we describe, roughly in order of increasing complexity, the series of tests used to evaluate the accuracy, repeatability and robustness of PLM when used to measure collagen fiber orientation of ocular tissues. Achilles tendon and silk were used as reference materials, as their fiber orientations are well known. Finally, we demonstrate the power of PLM by imaging a whole-globe section. Image processing and analyses were done using standard and custom code in Fiji [30].

2.1 Sample preparation

Fresh eyes and Achilles tendons from two years old healthy sheep were obtained from a local slaughterhouse and processed within 8 hours of death. The eyes were cannulated through the anterior chamber and intraocular pressure set using a fluid column to either a low (0 or 5 mmHg) or high (50 mmHg) pressure (normal sheep intraocular pressure is 10-15 mmHg [31]). The eyes were then immersion fixed with 10% formalin overnight while maintaining intraocular pressure. The anterior poles were excised with a razor and cryosectioned sagittally into 30 μm thick sections. The posterior poles were excised using an 8 mm trephine and cryosectioned coronally into 30 μm thick sections. One eye was cryosectioned sagittally whole, into 30 μm thick sections. Note that no labels or stains were applied to the eye tissue sections.

The tendons were loaded longitudinally using clamps affixed to a set stretch within the linear region of the loading profile (i.e. after the toe-region from collagen fibers straightening or uncrimping and before failure) [32]. After allowing for equilibration in the loaded condition for one hour in phosphate buffered saline (PBS), the PBS was replaced with 10% formalin and left overnight to fix. The tissue was cryosectioned into 50 μm thick longitudinal sections. One slide was dehydrated using ethanol, stained with hematoxylin and eosin (H&E), and mounted with xylene.
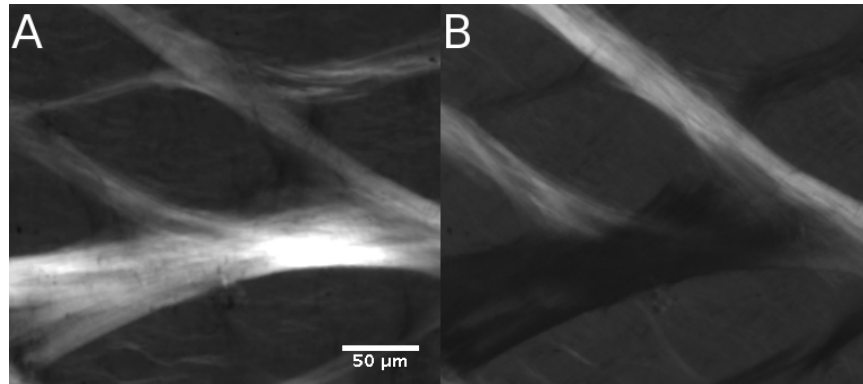

Fig. 1. Example polarization microscopy images of sheep lamina cribrosa trabeculae. The images were acquired with two different filter setups (A and B) differing by a 45° rotation. Although the trabecular structure of the lamina cribrosa is discernible in both images, the intensity varies with the relative orientation of the fibers and the filters.
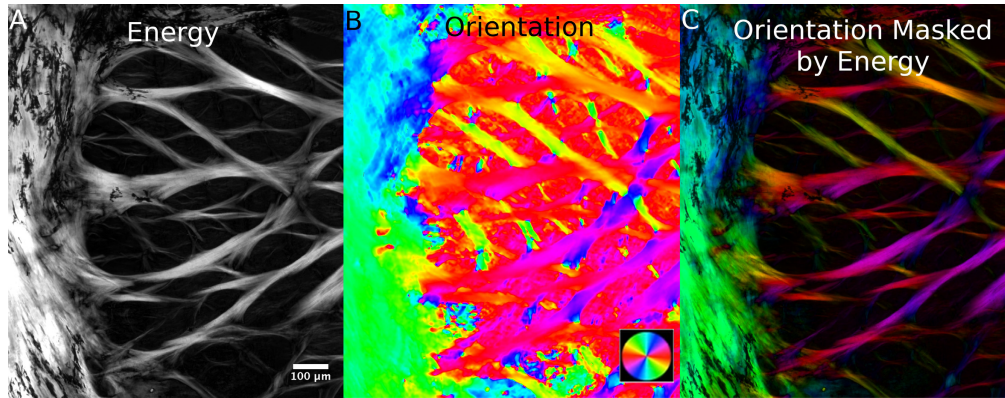
Fig. 2. Example results in a region of the peripheral lamina cribrosa and sclera. The main output from our technique was a local (pixel) measure of orientation (B). In a direct plot of orientation it is difficult to distinguish the structures of interest. To improve visualization, we also computed for each pixel the energy, as defined in the main text (A). The energy was then used to scale the brightness of the orientation maps producing an image of orientation "masked by energy" (C). This image allows easily discerning the trabecular structure of the lamina cribrosa simultaneously with the collagen fiber orientation. For clarity, all other orientation images in this manuscript are shown masked. Analyses were done with unmasked orientations.

2.2 Imaging and visualization

Tissue samples were imaged using standard bright-field imaging as well as PLM according to the protocols described by Kalwani and colleagues [23]. Briefly, a white light source and two polarizing filters were used (Hoya, Tokyo, Japan). The light passed through a polarizer, the sample, and an analyzer. A birefringent material, such as collagen, alters the polarization state of the light, resulting in increases or decreases of the light intensity observed after the analyzer depending on the relative orientation between the sample and the filters (Fig. 1). Multiple images were acquired with various filter orientations relative to the sample separated by 45°. The images were registered and the signal intensities from the multiple images were used to compute local orientation at each pixel [23]. For visualization, the fiber orientation at each pixel was also weighted by a parameter we denoted "energy" (Eq. (1)):

$$energy^2 = (I_{90} - I_0)^2 - (I_{135} - I_{45})^2 \qquad (1)$$

where I_α is the pixel intensity at an angle α to the analyzer direction (Fig. 2). Energy is thus large when there is a substantial change in signal with angle, and zero when there is no change, such as outside of the tissue.

To increase generality, we evaluated PLM with two microscope-camera pairs. For an Olympus BX60 microscope (Olympus, Tokyo, Japan) with a SPOT camera (SPOT Imaging Solutions, Sterling Heights, MI), image resolution was 1.48 µm/pixel using the 4x objective (NA 0.13) and 0.73 µm/pixel using the 10x objective (NA 0.3). For an Olympus SZX16 microscope with an Olympus DP80 camera and 0.8x objective (NA 0.12), image resolution was 0.37 µm/pixel with the 11.5x magnification setting and 4.4 µm/pixel with the 1x magnification setting.

2.3 Accuracy in tendon, single fibers, and cornea

We evaluated the accuracy by comparing the PLM measurements of fiber orientation with those from manual tracings. Manual tracing is a relatively common method used to determine fiber orientation in soft collagenous tissues [33–35], and permits comparing with a reference set by an expert. We conducted three test cases: loaded tendon fibers, a single curved silk fiber, and a sample of cornea from an eye at high intraocular pressure.
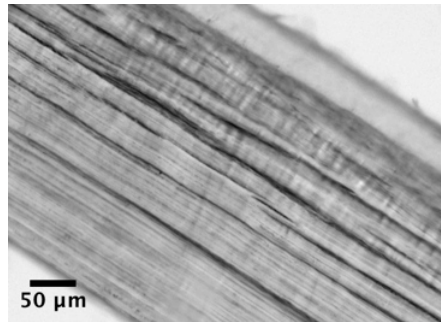
Fig. 3. Image of a sagittal section through the cornea of an eye fixed at 50mmHg. Analysis focused on the inner cornea region where the fibers displayed least undulations (bottom left).

In the first and simplest case, Achilles tendon fibers were straightened, as described in Section 2.1 above. A section through central tendon was imaged using the Olympus 10x objective. Manual measurements of the fiber orientation were obtained using 20 straight lines 6-16 μm long tracing the fibers of the tendon, and compared pixel-by-pixel with the fiber orientation determined using PLM. Absolute error was defined as the absolute difference between the manual and automated measurements. To account for systematic errors from manual tracing, we also calculated the relative error, which we defined as the difference between the automated measurements for a trace and the mean of those measurements along that trace. In straight fibers, as long as the trace is made in the same fiber, the measurements should be the same, and therefore, large variations were considered as errors by PLM.

In the second test, we placed a single curved silk fiber onto a glass slide, allowing it to rotate freely to release torsional stresses, and imaged it using the Olympus 10x objective. One long spline trace of the fiber was used, and the interpolated angle of the spline was compared to the automated orientation calculated by PLM at all pixels along the trace. The absolute and relative errors were calculated as above.

The third case replicated the first test, using corneal tissue. We selected a region through the central inner cornea of an eye fixed at 50 mmHg intraocular pressure, to reduce the effects of collagen undulations, or crimp [36], or of transverse fibers at odd angles [37] and imaged it using the Olympus 10x objective (Fig. 3). Similar to the first test, 20 manual straight-line traces were used. The cornea traces were 5-20 μm long. Once more, the absolute and relative errors were calculated as above.

For all three tests, Bland-Altman plots were also constructed to check for agreement between the marking and the PLM calculations (see Appendix Fig. 12).

2.4 Repeatability accounting for common variations in the imaging protocol

Next, we evaluated the repeatability of PLM using sheep optic nerve head tissue, which is more challenging due to the complexity of the architecture, the multiple fibers packed together, and the range of fiber densities. We evaluated the repeatability under three potential sources of variation that can cause artifacts: magnification [38], mosaic stitching [39], and tight fiber packing [40]. We selected and imaged a section through the lamina cribrosa of an eye fixed at high 50 mmHg intraocular pressure using Olympus 4x and 10x objectives. Images using the 10x objective were captured in a 2x2 mosaic (~20% overlap) to cover the same tissue region as with the 4x objective, and to evaluate the effects of stitching. Three image sets were acquired with each objective, yielding three measures of orientation at each pixel for each magnification. To determine repeatability, we registered the images of a given magnification and calculated at each pixel the fiber orientation difference between the orientation in that image and the mean pixel orientation across the three image sets at that magnification. To identify any potential effects of magnification, we compared the automated fiber orientation measurements between images acquired using the Olympus 4x and 10x

objectives. Some current techniques for quantifying local connective tissue orientation are affected by tissue density [7, 14]. Hence, we also split the data into sparse (lamina cribrosa beams) and dense (sclera) collagen fibers by manually segmenting the regions. To ascertain where the measurements were most variable, we also constructed images of the fiber orientation of the 3 trials using orientation lines for a visual representation of the fiber orientation differences. These lines were computed as the mean orientation over a region 12 μm in diameter.

2.5 Robustness to sample translation and rotation

Our next experiment evaluated the robustness of PLM to sample translations and rotations using optic nerve head tissue from eyes at low intraocular pressure. This is a more challenging test than those above because at low intraocular pressure the collagen fibers are crimped or wavy. Measurements of these micron-scale variations in fiber orientation are more sensitive to changes in image orientation and translation. A section through the lamina cribrosa was selected and imaged using the Olympus 10x objective. Between each image set acquisition, the sample was rotated 5° and translated. The translations were random in the plane of the sample, while still allowing a small area of interest to remain within the field of view. We acquired a total of 19 image sets, each at a different angle between 0° and 95°. As a measure of robustness we compared the sample orientation change with the change measured using PLM. Only areas that overlapped in all 19 image sets were analyzed. The whole area of overlap on all images was analyzed, including areas with pigment. Pigment can be a problem for other methods currently used for fiber orientation quantification because it absorbs light reducing signal and causing artifactual edges [41].
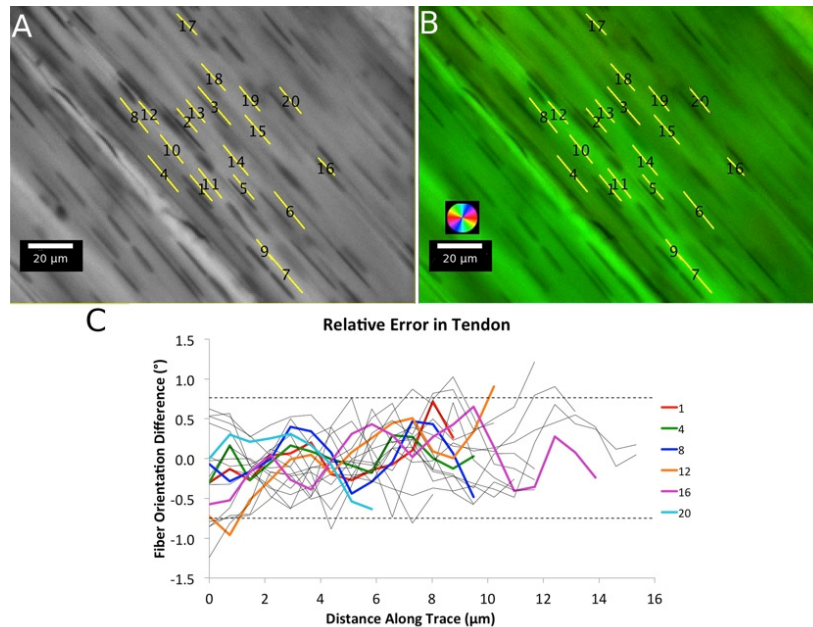

Fig. 4. Accuracy in loaded tendon tissue. Using images of loaded tendon (A), we compared PLM orientation (B) with orientation of manual traces. The relative error was small for all 20 traces (C). For clarity, six traces were highlighted in color, with the rest shown in grey. The dotted lines represent the 2.5th and 97.5th percentiles of the orientation differences.
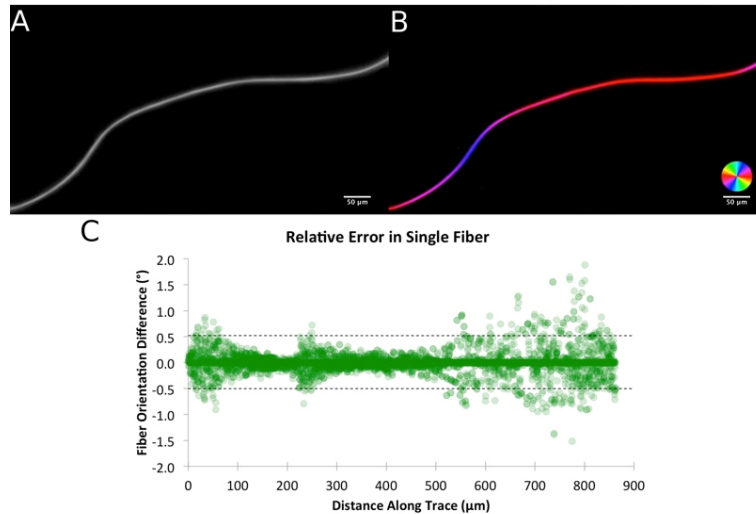
Fig. 5. Accuracy in a single curved silk fiber. Using images of a single curved silk fiber (A), we compared PLM orientation (B) with the interpolated orientation along a curved manual trace. The relative error was small along the entire trace (C). The dotted lines represent the 2.5th and 97.5th percentiles of the orientation differences.
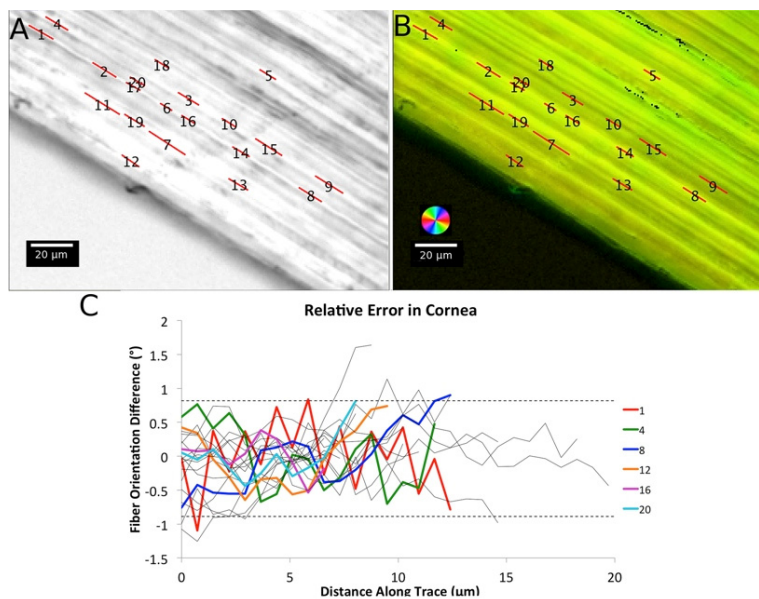

Fig. 6. Accuracy in pressurized corneal tissue. Using images of pressurized corneal tissue (A), we compared PLM orientation (B) with orientation of manual traces. The relative error was small for all 20 traces (C). For clarity, six traces were highlighted in color, with the rest shown in grey. The dotted lines represent the 2.5th and 97.5th percentiles of the orientation differences.

2.6 Robustness to tissue fixation

Formalin fixation has been shown to affect optical polarization properties of myocardium and liver samples [42], and therefore fixation could affect our measurements in ocular tissues. To quantify the effects of formalin fixation on PLM-measured fiber orientation we used the following experiment: a fresh sheep eye was cryosectioned sagittally into 30 μm thick sections. The unfixed sections were placed on glass slides and equatorial sclera was imaged

with PLM (SZX16 microscope, 11.5x magnification setting, 0.8x objective), before and after immersing the section in 10% formalin for 1 hour. We then quantified the differences in local fiber orientation before and after fixation.

2.7 Demonstration of PLM over the globe

We demonstrate the power of the technique over a broad field of view by imaging and analyzing an axial section of a whole sheep eye (~3 cm in diameter) fixed at 0 mmHg (SZX16 microscope, 1x magnification, 0.8x objective). We found this image to be clearest when masked by retardance [23].

3. Results

3.1 Accuracy in tendon, single fibers and cornea

For the loaded tendon case (Fig. 4) the average absolute error was 0.9°. The relative error had a standard deviation of 0.4° with 95% of the PLM measurements within 0.8°. For the single curved silk fiber (Fig. 5), the average absolute error was 4.5°. The relative error had a standard deviation of 0.2° with 95% of PLM orientation measurements within 0.5°. For the cornea at high intraocular pressure (Fig. 6), the average absolute error was 1.5°. The relative error had a standard deviation of 0.4° with 95% of the PLM measurements within 0.8°. Overall the absolute error was under 5°, and after accounting for systematic error, relative errors were under 2°. Images were acquired in less than a minute, and PLM analyzed in a few seconds.
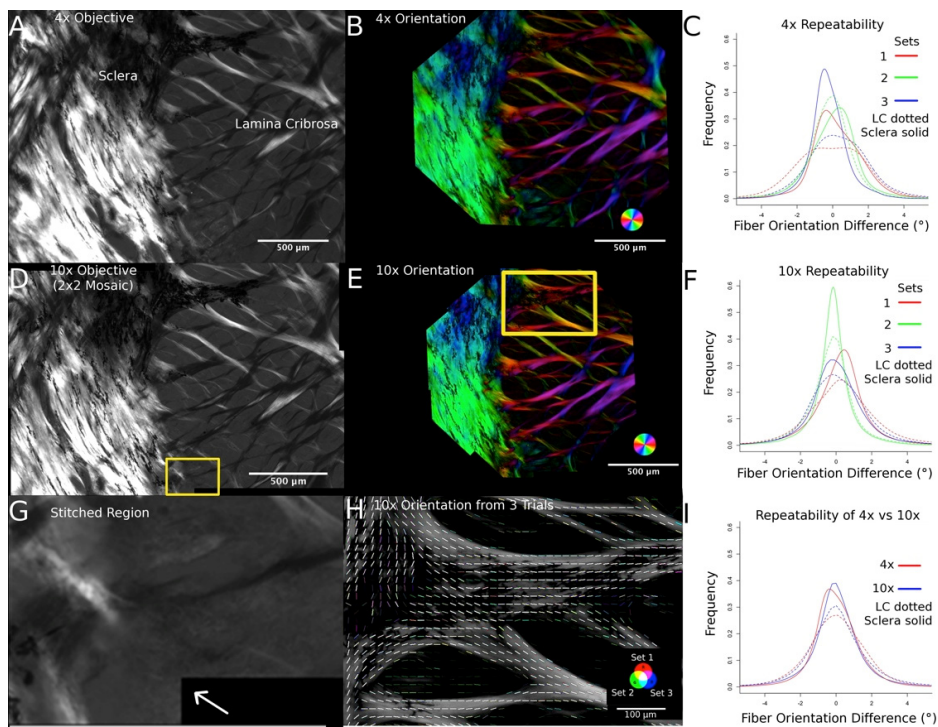

Fig. 7. Repeatability in optic nerve head tissue. Three image sets were captured using 4x and 10x objectives of a section of sheep optic nerve head tissue (A and D) and for each image set, the fiber orientation was calculated (B and E). The measurements were highly repeatable regardless of resolution (I) and tissue density (C and F) and there were no stitching artifacts (arrow in G indicates stitched region). The frequencies in panels C, F and I have been normalized to the total number of measurements. The fiber orientations from each image set were color coded and compared such that white indicated perfect agreement, and colors represented differences. The majority of the orientation lines are white (H).
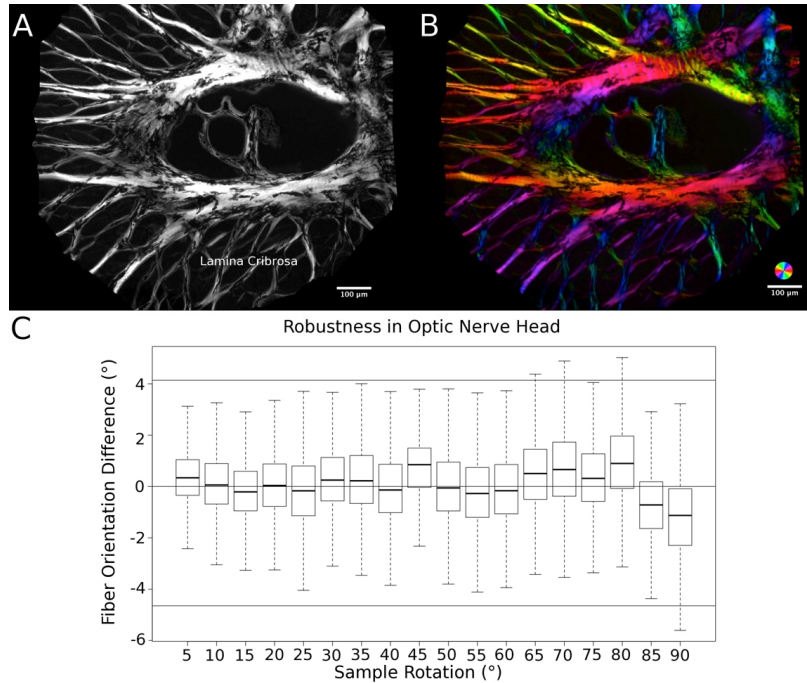
Fig. 8. Robustness in optic nerve head tissue. Image sets of sheep lamina cribrosa were taken (A) and for each set the fiber orientation was calculated (B) (see Visualization 1). The tight distributions through the different sample rotations show that our measurements are highly robust (C). The solid lines above and below represent the 2.5th and 97.5th percentiles of the orientation differences.
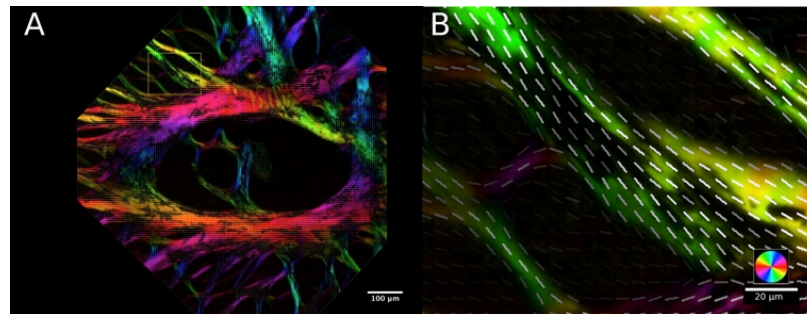

Fig. 9. Using polarization microscopy in areas of low energy. Shown is a region of the central lamina cribrosa (A), and a close-up of a couple of laminar beams with pigment (B). For clarity, in addition to color, orientation is also displayed with white lines. These lines represent the mean orientation in a square region centered at the line mid-point with size equal to half the line length. The orientations look reasonable and smooth, indicating that PLM is robust despite regions of low energy.

3.2 Repeatability accounting for common variations in the imaging protocol

For the pressurized sheep optic nerve head, measurements were highly repeatable, even when accounting for variations between magnifications, potential stitching artifacts, and varying tissue density (Fig. 7). For the images taken with the Olympus 4x objective, we found that 95% of the variability was within 3.5° (Fig. 7(A), 7(B), 7(C)), and for stitched images taken with the Olympus 10x objective, 95% of the variability was within 4.2° (Fig. 7(D), 7(E), 7(F)). Both magnifications had very similar fiber orientation variability distributions (Fig. 7(I)), demonstrating high repeatability across resolutions, without visible stitching artifacts in

the 2x2 stitched mosaic (Fig. 7(G)). The orientation lines showed very few differences. When there were differences, the magnitude of the differences was small (Fig. 7(H)). Repeatability was high regardless of tissue density. We found that for the sparser tissue, (lamina cribrosa), the 95% of the variability was within 4.6°, whereas for the denser tissue (sclera), it was within 1.9° (Fig. 7(C), 7(F)).

3.3 Robustness to sample translation and rotation

The measurements for the unloaded optic nerve head were robust to sample translation and rotation. For each of the sample translation and rotations, the mean and standard deviation of the error was calculated. From these 18 error distributions, the maximum mean error was 1.1° and the maximum standard deviation of 2.9°. When pooling the error distributions, 95% of the error was within 4.7° (Fig. 8) Even in areas with pigment on the lamina beams (Fig. 9) [43], the calculated orientations were smooth and continuous with adjacent unpigmented regions, demonstrating that the method was robust and produced satisfactory results.

3.4 Robustness to tissue fixation

The fiber orientation measurements were robust to formalin fixation (Fig. 10), with differences between fresh and 1 hour fixing of 0.58° (mean), 0.61° (median) and 2.4° (SD).

3.5 Demonstration of PLM over the globe

The fiber orientation was calculated using PLM over a whole globe axial section (Fig. 11).
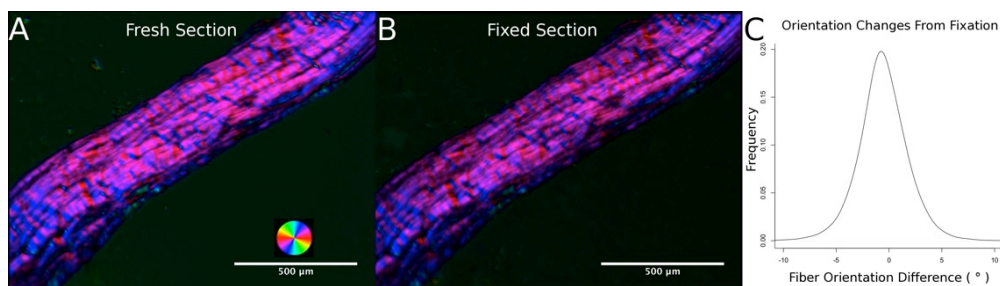

Fig. 10. PLM Images of PLM-determined fiber orientation of equatorial sclera fresh (A) and after 1 hour fixation in 10% formalin (B). Orientations were compared at every pixel within the tissues (C).

4. Discussion

We have demonstrated that PLM is a powerful technique for the study of ocular tissues, producing accurate, repeatable and robust measurements of collagen fiber orientation at micron-scale over cm-scale regions, which were not affected by formalin fixation. The measurements were obtained quickly and without the need for subjective manual tracings, or potential artifacts from staining, labeling or pigment. These results are important for the broad range of applications in which it is necessary to characterize the collagen structures of the eye, from fundamental understanding of eye physiology, to insight into the causes and changes associated with pathology and transplants.

PLM measurements of collagen fiber orientation were highly accurate, with 95% of the differences to manual tracings within 1°, and worst-case-scenario absolute differences under 5°. These differences are on the order of the repeatability in manual tracings. Differences could also be due to fiber torsion, or sub-fiber structures [44], that are detected by PLM orientation but indistinguishable for tracing. PLM measurements were also highly repeatable, with 95% of the differences between sessions under 4°, across magnifications and mosaic stitching. Repeatability becomes increasingly challenging at higher magnifications as finer details of the structure become distinguishable, which must be consistent across images. Our

method had slightly worse repeatability in higher magnification images, but measurements were still highly repeatable. Stitching artifacts can occur with image problems such as high noise, imperfect calibration, poor or irregular focus, or lack of consistent illumination. Our stitched mosaics had no noticeable edges, making for seamless mosaics, greatly extending the regions that can be analyzed from the relatively small field of view of a single image.
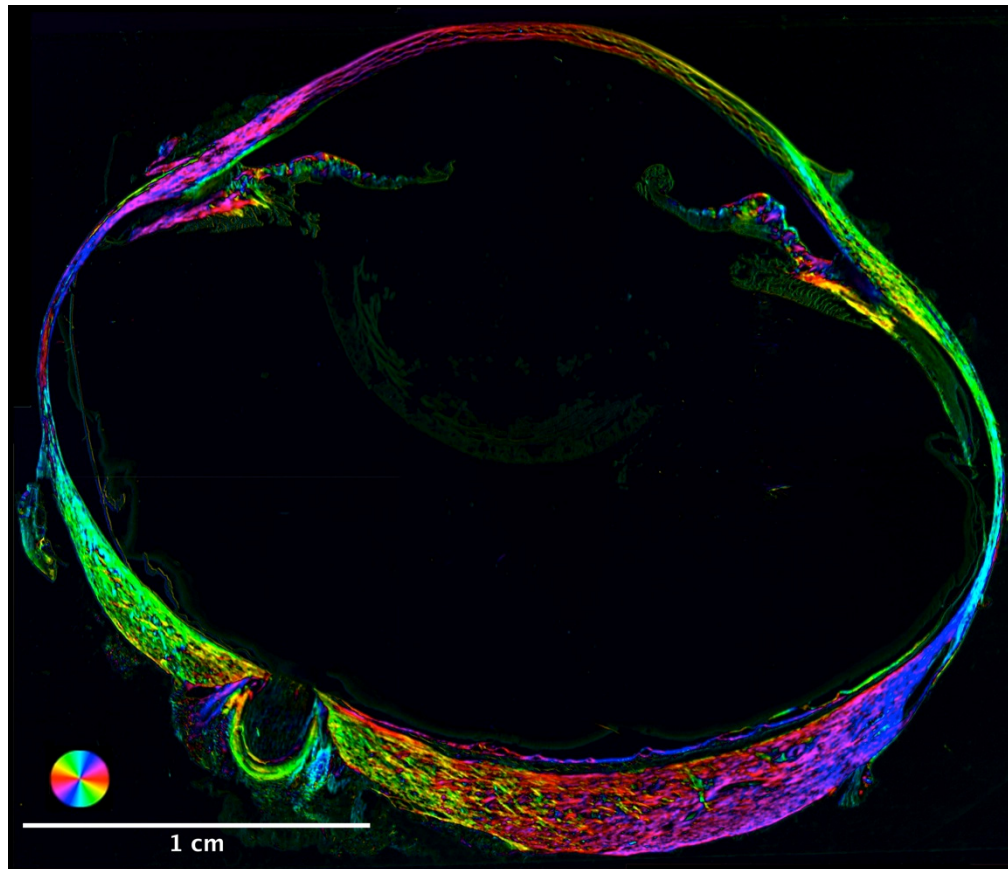

Fig. 11. PLM image of a whole-globe axial eye section. This image demonstrates the objective quantification of collagen fiber orientations over a broad field of view.

Accuracy and repeatability were not affected by collagen density, producing similarly reliable results in sparse regions, like the lamina cribrosa, and dense regions, like the sclera. Whereas other techniques of fiber analysis are challenged by either low [7] or high [14] collagen densities, PLM can be used to do fair comparisons independent of density.

PLM measurements were robust to sample translation and rotation as well as formalin fixation, with differences in fiber orientation only slightly larger than repeatability. Small fixation effects were expected since immersion of the section in fixative may cause slight tissue displacement, deformation and shrinkage [42].

There is a growing number of techniques for characterizing collagen fiber architecture of ocular tissues at the micro-scale. For many years, the most common techniques relied on visual inspection of tissue sections [45]. In addition to being subjective and slow, these techniques required tissue dehydration, staining and/or labeling which add variability and affect the measurements badly due to shrinkage. PLM, does not require processing the tissue in these ways, and is therefore more likely to have high fidelity. Further, sections imaged with

PLM remain available for other work. For example, labeling to confirm the type of collagen [46].

In recent years, nonlinear microscopy has become increasingly common for the study of collagen architecture at the micro-scale, in large part due to the power of optical sectioning not available in our implementation of PLM [27, 47]. After imaging, fiber orientation is obtained through either manual tracings [35] or some form of an intensity-based method such as gradient, edge-detection, Fourier analysis, and others [41, 48]. Intensity-based methods, while not subjective or as slow as manual tracings, have important downsides compared with PLM. Most notable is that fiber orientations can only be reliably quantified when the fibers can be clearly distinguished from one another. Hence, the effectiveness of intensity based methods decreases when the tissues are dense, when the edges of fibers cross or overlap, or in any situation where the visible edges do not represent the true orientation of the underlying collagen, such as when there is fiber torsion or twist, or fiber fractures. To reduce these problems, intensity based methods typically require higher magnifications, and much longer imaging times, than PLM. Intensity based methods also produce invalid results within or near pigment. This is important because pigments are common in several species of interest in ophthalmology research, such as non-human primates, pigs, sheep and rats. Due to the high absorbance, pigments also increase the risk of thermal damage to the tissues. In contrast, PLM measurements are objective, fast, without the risk of thermal damage and often producing excellent results even through pigmentation. Further, through energy, PLM provides a measure of signal at a pixel, which can be used to estimate the quality of a local measure.

There is also great interest in characterizing ocular collagen architecture at large scale, and several techniques have been developed to this effect, including small-angle light scattering [7, 8], small angle x-ray scattering [7, 49], and wide angle x-ray scattering (WAXS) [10]. WAXS has recently been applied to the whole eye [50]. Like PLM, these methods are based on the molecular characteristics of collagen. However, these methods have substantially worse resolutions than PLM. For example, measurements using small angle light scattering had 300-500 µm transverse resolution [8], which is insufficient to capture the details of lamina cribrosa architecture. Depth resolution is also usually worse than for PLM, with noise and other problems worsening as the sample thickness decreases, such that the detriments are already substantial even for a relatively thick 50 µm thick sample [7]. We have shown transverse PLM resolutions on the order of 1 µm/pixel. Depth resolution in our PLM implementation is set by the thickness of the histological sections, in this study of 30 µm. In preliminary studies (data not shown) we have obtained excellent results for untreated sections as thin as 8 µm, and in 1 µm-thick sections treated with picrisirius red (to enhance collagen birefringence). Synchrotron radiation has also been used to acquire micron-scale resolution data from ocular tissues [12, 28], but the super-specialized equipment needed makes it less widely available than PLM.

By enabling fast measurement at both macro and micro-scales, PLM promotes a multi scale characterization of ocular tissues, averting the problems of having to combine data from disparate imaging modalities, which typically have different limitations and are therefore not well suited for superposition.

It is important to consider the limitations of PLM and our analysis in this work. The orientation data obtained is only on the plane of the section, two-dimensional, while the architecture of collagen fibers in ocular tissues is three-dimensional. This limitation, however, is shared by most methods used to characterize ocular collagen. Often, methods that can, in theory, provide three-dimensional information, such as nonlinear imaging, are still used in two-dimensions due to the complexities of the tissue [10, 51]. Also, the orientation data obtained from our PLM at each pixel represents the predominant fiber orientation at that point. It is possible that several fibers with various orientations pass through a pixel, especially at the lower magnifications. Use of thinner sections would reduce this effect.

Another limitation is the use of tissue sections, which can introduce artifacts due to warping. These effects can be reduced by the use of unwarping techniques using embedded fiducial markers [52]. Finally, we obtained good data from both microscope-camera setups, but we did not directly compare these and it is possible that the choice of camera can affect the measurements. Considering the above, we note that we see PLM as complimentary to scattering-based techniques, which have tremendous potential in ophthalmology due to their ability to obtain data from thick samples.

5. Conclusions

We have demonstrated that PLM enables a fast, objective, accurate, precise, repeatable and robust multi-scale characterization of collagen fiber orientation in ocular tissues, without the need for tissue dehydration, labeling or staining. This fiber orientation information has powerful applications in ophthalmology, including understanding the role of collagen architecture in normal physiology and aging, as well as in pathology.
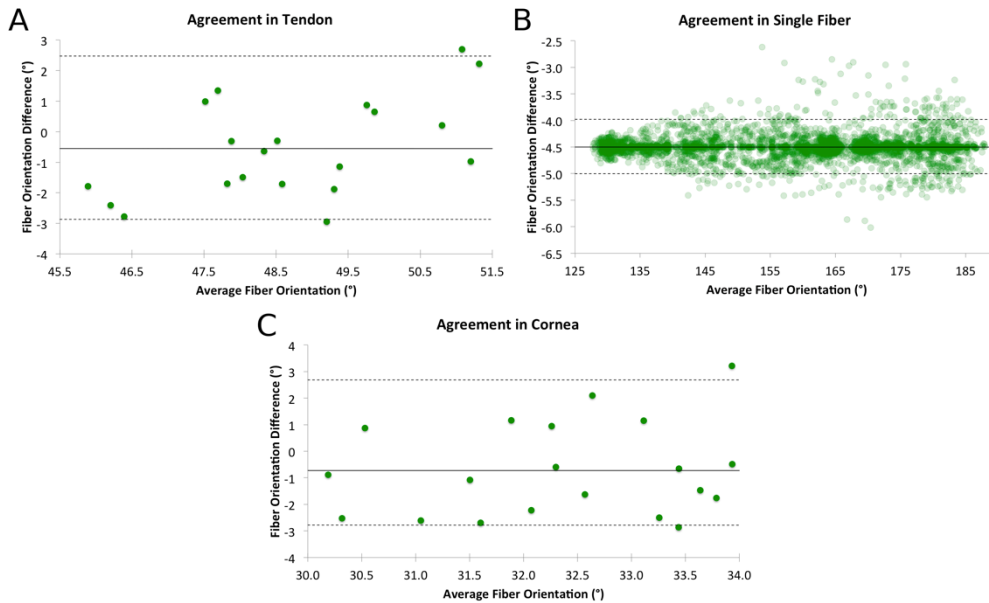
6. Appendix

Fig. 12. Bland-Altman plots of the agreement between manual markings and PLM orientation measurements in tendon (A), a single curved fiber (B), and cornea (C). For the tendon and cornea tests, the mean PLM orientation for each line was used to construct the plot whereas every point was used for the single fiber. The dotted lines represent the 2.5th and 97.5th percentiles of the orientation differences. We note that since our goal was to determine whether the two measurement methods (manual and PLM) produced the same results, a mixed effects model was not the appropriate analysis tool. Using a mixed effects model would have required us to define apriori a criteria for measurements to be the same. Instead of making such an arbitrary call, we present the results as obtained and show agreement.